Materials Research Bulletin 91 (2017) 77–84

Contents lists available at ScienceDirect

Materials Research Bulletin

journal homepage: www.elsevier.com/locate/matresbu

Multicolor upconversion emission of lanthanide-doped single $LiYF_4$ and $LiLuF_4$ microcrystal

Wei Gao[a], Jun Dong[a], Zhaojin Wang[b], Zhenglong Zhang[b], Hairong Zheng[b,*]

[a] School of Electronic Engineering, Xi'an University of Post & Telecommunications, Xi'an 710121, PR China
[b] School of Physics and Information Technology, Shaanxi Normal University, Xi'an 710062, PR China

ARTICLE INFO

Article history:
Received 13 November 2016
Received in revised form 20 March 2017
Accepted 21 March 2017
Available online 23 March 2017

Keywords:
Single microparticle
Selective excitation
Optical materials
Optical properties
Luminescence

ABSTRACT

Yb^{3+}/Ln^{3+} co-doped $LiYF_4$ and $LiLuF_4$ microcrystals (MCs) are synthesized by a facile hydrothermal method. The upconversion (UC) luminescence properties of single $LiYF_4$ and $LiLuF_4$:Yb^{3+}/Ln^{3+} MC are studied by a confocal microscopy setup under NIR 980 nm laser excitation. The single $LiLuF_4$ MC displays stronger UC emission intensity than that of single $LiYF_4$ MC, which is due to the varied site symmetry of the crystal field. The possible UC mechanism, the influence of surface properties and excitation positions on the UC luminescence emission are also investigated. Investigating the luminescence properties of a single particle can effectively avoid environmental influence, achieve selective targeting excitation, and provide precise information for studying the luminescence mechanism of Ln^{3+} ions.

© 2017 Published by Elsevier Ltd.

Given their superior optical properties, lanthanide (Ln^{3+})-doped luminescence materials, such as oxides [1,2], fluorides [3,4], phosphates [5], and vanadates [6], have been used as phosphors in lighting and used in the development of new laser crystals, optical storage and amplifiers, and fluorescent imaging of cancer cells and solar cells [7-11]. Among diverse host materials, rare-earth (RE) fluoride compounds, $AERF_4$ (A = alkali metal) usually exhibit strong UC emission because of low phonon energy, which can effectively decrease nonradiative relaxation rates [12,13]. Up to now, the hexagonal phase $NaYF_4$ crystal is considered to be the most efficient UC host material [14,15]. Many reports exist about RE-doped $NaYF_4$ nano- or microcrystals in the past few years [16–19]. However, as another important fluoride UC host material, $NaLuF_4$ host also displays excellent UC emission behavior due to structure similarity to $NaYF_4$ and advantageous ionic distance. The Lu^{3+} (0.085 nm) ionic radius is much closer to that of the Yb^{3+} (0.086 nm) ions than the Y^{3+} (0.089 nm) ions [20]. Therefore, Lu-based fluorides should be more stable for doping of Yb^{3+} ions with a high concentration and achieve efficient energy transfer between the ions. Recently, Qin's and Li's groups have confirmed that the UC emission intensities of RE-doped $NaLuF_4$ crystals are stronger than that of $NaYF_4$ crystals [21,22]. The same as $NaYF_4$, the $LiYF_4$ crystals with tetragonal scheelite structure are also considered to be one of the excellent host materials for RE ion-doped UC luminescence [23–25]. Recently, many different synthesis methods have been employed to obtain the $LiYF_4$ crystal, including hydrothermal method, thermal decomposition, and surfactant-free molten salt method [26–28]. The total UC quantum yield of $LiYF_4$:Er^{3+} nanocrystals is almost four times higher than that of $NaYF_4$:Yb^{3+}/Er^{3+} nanocrystals under 1490 and 980 nm excitation, respectively [29]. Liu's group has reported that $Yb^{3+}/(Er^{3+}$, Tm^{3+}, $Ho^{3+})$-doped $LiYF_4$ nanocrystals show superior UC fluorescence [30]. Meanwhile, our group has also synthesized $LiYF_4$:$Yb^{3+}/(Er^{3+}$, $Pr^{3+})$ microcrystals (MCs) and obtained strong UC luminescence [31–33]. Similar to $NaLuF_4$ crystal, the $LiLuF_4$ crystal would become a potential UC emission host material. However, to the best of our knowledge, the study of optical properties of $LiLuF_4$ MCs has been barely reported before, especially for single $LiLuF_4$ MC [34].In this work, $LiYF_4$:Yb^{3+}/Ln^{3+} MCs are synthesized via a facile hydrothermal method with EDTA as a chelating agent. The $LiLuF_4$:Yb^{3+}/Ln^{3+} MCs have been attempted to be prepared through the same method with $LiYF_4$ MCs. The UC luminescence properties of single $LiYF_4$ and $LiLuF_4$ MC are carefully studied by a confocal microscopy setup under 980 nm laser excitation. In addition, the UC emission intensity of the different parts of single $LiYF_4$ MCs is discussed in detail. The UC emission mechanisms are investigated based on the emission spectra.

* Corresponding author.
E-mail address: hrzheng@snnu.edu.cn (H. Zheng).

http://dx.doi.org/10.1016/j.materresbull.2017.03.043
0025-5408/© 2017 Published by Elsevier Ltd.

1. Introduction

Given their superior optical properties, lanthanide (Ln^{3+})-doped luminescence materials, such as oxides [1,2], fluorides [3,4], phosphates [5], and vanadates [6], have been used as phosphors in lighting and used in the development of new laser crystals, optical storage and amplifiers, and fluorescent imaging of cancer cells and solar cells [7–11]. Among diverse host materials, rare-earth (RE) fluoride compounds, $AERF_4$ (A = alkali metal) usually exhibit strong UC emission because of low phonon energy, which can effectively decrease nonradiative relaxation rates [12,13]. Up to now, the hexagonal phase $NaYF_4$ crystal is considered to be the most efficient UC host material [14,15]. Many reports exist about RE-doped $NaYF_4$ nano- or microcrystals in the past few years [16–19]. However, as another important fluoride UC host material, $NaLuF_4$ host also displays excellent UC emission behavior due to structure similarity to $NaYF_4$ and advantageous ionic distance. The Lu^{3+} (0.085 nm) ionic radius is much closer to that of the Yb^{3+} (0.086 nm) ions than the Y^{3+} (0.089 nm) ions [20]. Therefore, Lu-based fluorides should be more stable for doping of Yb^{3+} ions with a high concentration and achieve efficient energy transfer between the ions. Recently, Qin's and Li's groups have confirmed that the UC emission intensities of RE-doped $NaLuF_4$ crystals are stronger than that of $NaYF_4$ crystals [21,22]. The same as $NaYF_4$, the $LiYF_4$ crystals with tetragonal scheelite structure are also considered to be one of the excellent host materials for RE ion-doped UC luminescence [23–25]. Recently, many different synthesis methods have been employed to obtain the $LiYF_4$ crystal, including hydrothermal method, thermal decomposition, and surfactant-free molten salt method [26–28]. The total UC quantum yield of $LiYF_4$:Er^{3+} nanocrystals is almost four times higher than that of $NaYF_4$:Yb^{3+}/Er^{3+} nanocrystals under 1490 and 980 nm excitation, respectively [29]. Liu's group has reported that Yb^{3+}/(Er^{3+}, Tm^{3+}, Ho^{3+})-doped $LiYF_4$ nanocrystals show superior UC fluorescence [30]. Meanwhile, our group has also synthesized $LiYF_4$:Yb^{3+}/(Er^{3+}, Pr^{3+}) microcrystals (MCs) and obtained strong UC luminescence [31-33]. Similar to $NaLuF_4$ crystal, the $LiLuF_4$ crystal would become a potential UC emission host material. However, to the best of our knowledge, the study of optical properties of $LiLuF_4$ MCs has been barely reported before, especially for single $LiLuF_4$ MC [34].

In this work, $LiYF_4$:Yb^{3+}/Ln^{3+} MCs are synthesized via a facile hydrothermal method with EDTA as a chelating agent. The $LiLuF_4$:Yb^{3+}/Ln^{3+} MCs have been attempted to be prepared through the same method with $LiYF_4$ MCs. The UC luminescence properties of single $LiYF_4$ and $LiLuF_4$ MC are carefully studied by a confocal microscopy setup under 980 nm laser excitation. In addition, the UC emission intensity of the different parts of single $LiYF_4$ MCs is discussed in detail. The UC emission mechanisms are investigated based on the emission spectra.

2. Experimental

2.1. Materials

All chemicals used in the current study are graded and are analytical used without further purification. $Y(NO_3)_3$, $Lu(NO_3)_3$, $Yb(NO_3)_3$, $Er(NO_3)_3$, $Tm(NO_3)_3$, $Ho(NO_3)_3$ and $Eu(NO_3)_3$ are obtained by dissolving Y_2O_3, Lu_2O_3, Yb_2O_3, Er_2O_3, Tm_2O_3, Ho_2O_3 and Eu_2O_3 (99.99%. Sigma-Aldrich) with nitric acid, respectively. NH_4F(98.0%), LiF(98.0%), and EDTA (ethylenediamine tetraacetic acid, 99.0%) with analytical grade are supplied by the Sinopharm Chemical reagent Co., Ltd.

2.2. Synthesis of $LiYF_4$:Yb^{3+}/Ln^{3+} and $LiLuF_4$:Yb^{3+}/Ln^{3+} MCs

Yb^{3+}/Ln^{3+} co-doped $LiYF_4$ and $LiLuF_4$ MCs are synthesized by hydrothermal method; the detailed process was via our previously reported procedure [32–34]. The preparation process is presented as follows if the synthesization of $LiYF_4$:20%Yb^{3+}/2%Er^{3+} MCs is taken as an example. First, 20.0 ml deionized water, 0.78 ml (0.5 M) $Y(NO_3)_3$, 0.20 ml (0.5 M)$Yb(NO_3)_3$, 0.02 ml (0.5 M) $Er(NO_3)_3$, and 0.93 g EDTA are mixed to form a chelate complex solution under vigorous stirring for 30 min. Second, 0.48 g LiF and 0.17 g NH_4F are added into the chelate complex solution. Then, stirring continued for about 20 min until it completely becomes a white liquid. Finally, the white liquid is slowly transferred into a 40 ml Teflon-lined autoclave and is heated at 220 °C for 48 h to obtain $LiYF_4$:20%Yb^{3+}/2%Er^{3+} MCs. The MCs are obtained by centrifuging and washing with deionized water and ethanol for several times. The collected samples are finally dried at 60 °C for 12 h. $LiLuF_4$:Yb^{3+}/Ln^{3+} MCs were prepared the same as the $Lu(NO_3)_3$, i.e., by replacing $Y(NO_3)_3$ into the precursor mixture under the same reactive conditions.

2.3. Sample characterization and spectral measurement

The crystal structure, morphology, size and composition of samples are characterized by a D/Max2550VB+/PC x-ray diffraction (XRD) meter and scanning electron microscope (SEM). Fourier transform infrared spectroscopy (FTIR) is measured with a Brucher EQUINX55 spectrometer using KBr pellets. For spectroscopic

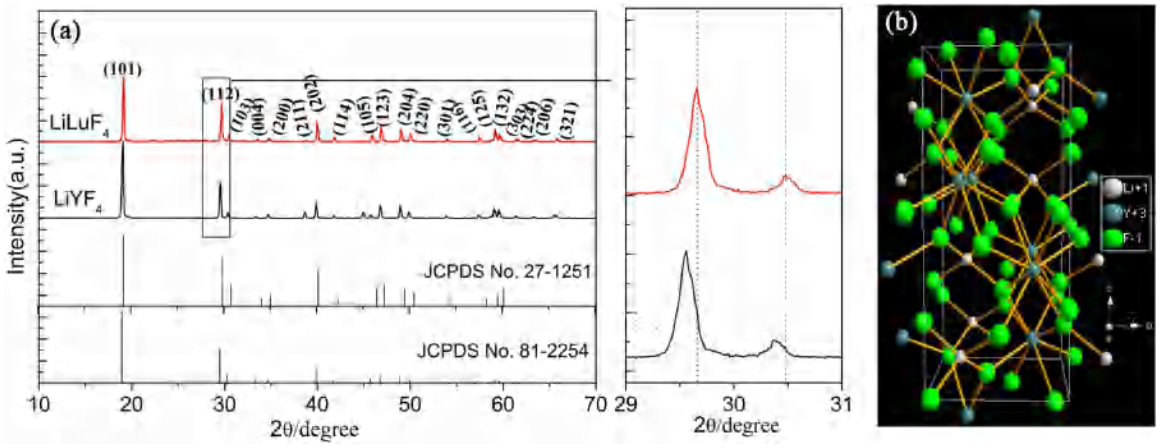

Fig. 1. (a) XRD patterns of the $LiYF_4$: 20%Yb^{3+}/2%Er^{3+} and $LiLuF_4$: 20%Yb^{3+}/2%Er^{3+} MCs. (b) Schematic illustrations of crystal structure of pure $LiYF_4$ MCs.

measurements, the semiconductor laser (MGL-III-532) and Ti sapphire laser (Mira-900) are employed as excitation sources. The spectrometer (SP2750i) with a spectral resolution of 0.008 nm is used for luminescence collection and detection. The optical microscope (OLYMPUS-BX51) is used for the confocal setup, and the corresponding magnifications are 100, 500 and 1000. Proper notch filters are placed in front of the entrance of the monochromator to block the scattering light. All of the spectroscopic measurements are carried out at room temperature.

3. Results and discussion

3.1. Crystal structure and morphology of $LiYF_4$ and $LiLuF_4$:Yb^{3+}/Ln^{3+} MCs

The typical XRD patterns of $LiYF_4$:20%Yb^{3+}/2%Er^{3+} MCs and $LiLuF_4$: 20%Yb^{3+}/2%Er^{3+} MCs are shown in Fig. 1(a). The strong and sharp diffraction peaks of $LiYF_4$:Yb^{3+}/Er^{3+} MCs and $LiLuF_4$:Yb^{3+}/Er^{3+} MCs can be clearly found, and the pure tetragonal phase (space group $I4_1/a$) with high crystallinity is confirmed, which are well-consistent with the standard JCPDS 81–2254 and JCPDS 27–1251 cards, respectively. The corresponding calculated lattice parameters for $LiYF_4$:Yb^{3+}/Er^{3+} MCs are $a = 5.167$ Å and $c = 10.721$ Å on the other hand, the calculated lattice parameters for $LiLuF_4$:Yb^{3+}/Er^{3+} MCs are $a = 5.124$ Å and $c = 10.537$Å, respectively. Owing to the likeness of ion radii among Y^{3+}, Lu^{3+}, Yb^{3+}, and Er^{3+} ions, the doping Yb^{3+} and Er^{3+} evidently have an effect on the $LiYF_4$ and $LiLuF_4$ structures. No other impurity peaks are detected. Additionally, all the diffraction peaks of $LiLuF_4$ MCs slightly shifted to larger diffraction angles, suggesting that the crystal unit cell shrinks after Y^{3+} ions were substituted by Lu^{3+} ($r_{Lu3+} = 0.085$ nm $< r_{Y3+} = 0.089$ nm) ions [20]. Fig. 1(b) shows the schematic crystal structure of $LiYF_4$. The Y^{3+} ion is coordinated by eight F^- ions and Li^+ is coordinated by four F^- ions; the F-Y bond lengths are 2.244 Å for four of the bonds and 2.297 Å for the other four Li-F. The unit cell contains 24 atoms. The valency, ionic radius, and charge compensation of Lu^{3+} are expected to substitute for the Y^{3+} ion site in $LiYF_4$ MCs. Thus, the structure of $LiLuF_4$ MCs is the same as that of $LiYF_4$ MCs.

Fig. 2 shows the SEM images of $LiYF_4$:Yb^{3+}/Er^{3+} and $LiLuF_4$:Yb^{3+}/Er^{3+} MCs. It can be observed that the $LiYF_4$:Yb^{3+}/Er^{3+} and $LiLuF_4$:Yb^{3+}/Er^{3+} MCs are all octahedral in shape; the average size is around 10 μm. Meanwhile, we are also able to find that $LiYF_4$:Yb^{3+}/Er^{3+} and $LiLuF_4$:Yb^{3+}/Er^{3+} MCs are highly uniform and regular with a smooth surface. The size and morphology of $LiYF_4$:Yb^{3+}/Er^{3+} MCs have no evident change when the Lu^{3+} ions completely replaced the Y^{3+} ions, owing to their similar ionic radius. The ionic radius of Tm^{3+} (0.087 nm) and Ho^{3+} (0.089 nm) are close to the Er^{3+} (0.088 nm) ionic radius [20]. Consequently, the XRD results and SEM images of $LiYF_4$ and $LiLuF_4$:Yb^{3+}/Tm^{3+}(Ho^{3+}) are similar to the LiY/LuF_4:Yb^{3+}/Er^{3+} in the Supporting information, as shown in Fig. S(1–3). The EDX spectra of $LiYF_4$:Yb^{3+}/Er^{3+} and $LiLuF_4$:Yb^{3+}/Er^{3+} MCs are shown in Fig. 2(c–d). The result indicates that the main elemental components of the samples are Y, Lu, Yb, F, and Er.

3.2. UC emission of Yb^{3+}/Ln^{3+} co-doped single $LiYF_4$ and $LiLuF_4$ MC

Fig. 3 displays the UC emission spectra; the peak area for the blue, green, and red emissions; and the corresponding CIE chromaticity diagram and luminescent photographs of Yb^{3+}/Ln^{3+}

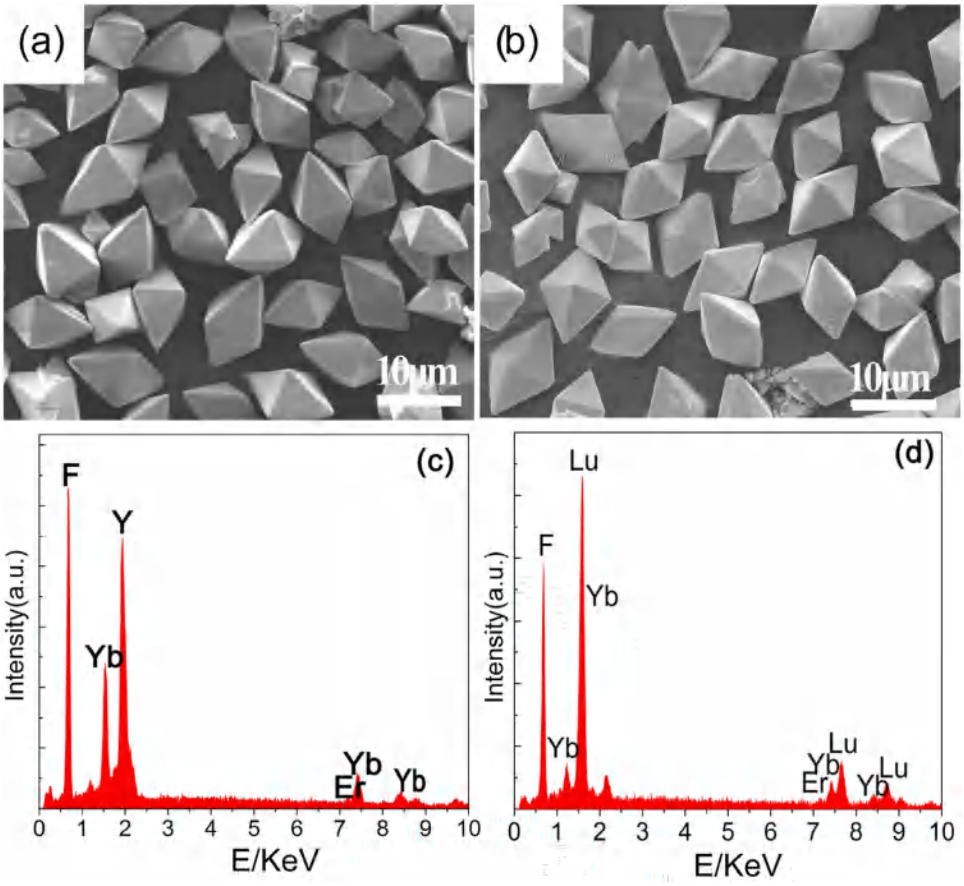

Fig. 2. SEM images and EDX spectra of (a) $LiYF_4$: Yb^{3+}/Er^{3+} and (b) $LiLuF_4$:Yb^{3+}/Er^{3+} MCs.

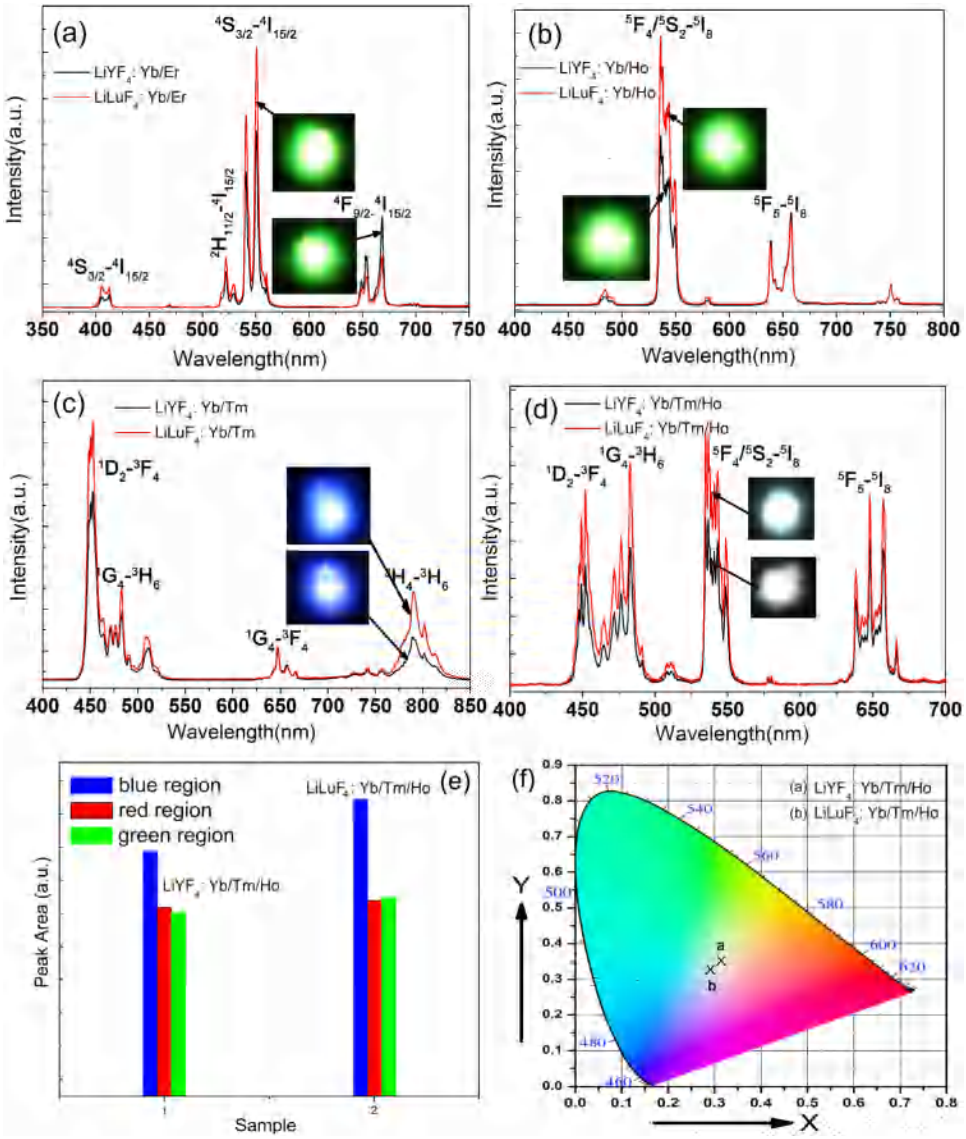

Fig. 3. (a–d) The UC emission spectra of single LiY/LuF$_4$: 20%Yb^{3+}/2%Ln^{3+}. (e) The relative peak area for the blue, green and red of single LiYF$_4$ and single LiLuF$_4$ MC. (f) The CIE chromaticity diagram of the single LiYF$_4$ and LiLuF$_4$ MC. (For interpretation of the references to colour in this figure legend, the reader is referred to the web version of this article.)

co-doped single LiYF$_4$ and LiLuF$_4$ MC by a confocal microscopy setup under 980 nm excitation. The schematic diagram of the luminescence spectroscopy test system is shown in Fig. S4. As shown in Fig. 3(a), an intense green (524 nm and 545 nm) emission is observed in the single LiYF$_4$: 20%Yb^{3+}/2%Er^{3+} and LiLuF$_4$:20%Yb^{3+}/2%Er^{3+} MC, which is assigned to the $^2H_{11/2}$/$^4S_{3/2} \rightarrow {}^4I_{15/2}$ and $^2H_{9/2} \rightarrow {}^4I_{13/2}$ transitions of Er^{3+} ions; the weak red (667 nm) emission is assigned to the $^4F_{9/2} \rightarrow {}^4I_{15/2}$ transition [35]. Fig. 3(b) displays the characteristic emission (green and red) peaks that are assigned to $^5S_2$/$^5F_4 \rightarrow {}^5I_8$ (540 nm) and $^5F_5 \rightarrow {}^5I_8$ (650 nm) transitions of Ho^{3+} ions in the single LiYF$_4$:20%Yb^{3+}/2%Ho^{3+} and LiLuF$_4$:20%Yb^{3+}/2% Ho^{3+} MC, respectively [36]. Some weak blue emission (484 nm) and NIR emission (750 nm) peaks can be also observed in Fig. 3(b), which are associated with the transition of $^5F_3 \rightarrow {}^5I_8$ and $^5S_2$/$^5F_4 \rightarrow {}^5I_7$ of Ho^{3+} ions, respectively. For the single LiYF$_4$:20%Yb^{3+}/2%Tm^{3+} and single LiLuF$_4$:20%Yb^{3+}/2% Tm^{3+} MC, the four obvious emission peaks at 453, 478, 650, and 800 nm can be attributed to $^1D_2 \rightarrow {}^3F_4$, $^1G_4 \rightarrow {}^3H_6$, $^3H_4 \rightarrow {}^3H_6$, and $^1G_4 \rightarrow {}^3F_4$ transitions of Tm^{3+} ions, respectively, as shown in Fig. 3(c) [37]. The UC emissions of the Yb^{3+}/Tm^{3+}/Ho^{3+} co-doped single LiYF$_4$ and LiLuF$_4$ MC are shown in Fig. 3(d). The blue (453 and 478 nm), green (540 nm), and red (650 nm) emissions can be observed. Compared with the UC emission of Yb^{3+}/Ho^{3+} and Yb^{3+}/Tm^{3+} co-doped single LiYF$_4$ and LiLuF$_4$ MC in Figs. 3(b) and (c), the origin of the observed emission peaks can be easily assigned, as shown in Fig. 3(d). The blue emission centered at 453 and 478 nm is generated from the $^1G_4 \rightarrow {}^3H_6$ and $^1D_2 \rightarrow {}^3F_4$ transitions of Tm^{3+} ions. The green and red emissions originate from $^5S_2$/$^5F_4 \rightarrow {}^5I_8$ (540 nm) and $^5F_5 \rightarrow {}^5I_8$ (650 nm) of Ho^{3+} ions. A very weak red emission (650 nm) can also be generated from $^1G_4 \rightarrow {}^3F_4$ transition of Tm^{3+} ions, which may be covered by the red emission of Er^{3+} ions. From the corresponding luminescent photographs in the inset of Fig. 3(a–d), it is found that 20%Yb^{3+}/2%Er^{3+}, 20%Yb^{3+}/2%Tm^{3+}, 20%Yb^{3+}/2%Ho^{3+}, and 20%Yb^{3+}/2%Tm^{3+}/2%Ho^{3+} co-doped single LiYF$_4$ and LiLuF$_4$ MC all exhibit bright green, blue, green, and white emissions, respectively. Moreover, the relative peak area for blue, green, and red of Tm^{3+}

and Ho^{3+} co-doped single $LiYF_4$ and $LiLuF_4$ MC are calculated as shown in Fig. 3(e). Obviously, the intensity of the three emission peaks is different, and the much stronger blue emission can be observed in the single $LiLuF_4$ MC. This finding indicated that the $LiLuF_4$ MC shows higher UC emission efficiency than that of the single $LiYF_4$. Fig. 3(f) shows the corresponding CIE chromaticity diagram; the CIE chromaticity coordinates of 20%Yb^{3+}/2%Tm^{3+}/2% Ho^{3+} co-doped single $LiYF_4$ (point a) and $LiLuF_4$ (point b) MC are determined to be $x = 0.31$, $y = 0.32$ and $x = 0.29$, $y = 0.32$, respectively. Thus, the output color of the single $LiYF_4$ MC is very close to the standard equal energy white illuminating light ($x = 0.33$, $y = 0.33$). Furthermore, the UC emission intensities of Yb^{3+}/Ln^{3+}-doped single $LiLuF_4$ MC are all stronger than that of the single $LiYF_4$ MC. And single $LiYF_4$: Yb^{3+}/(Er^{3+}, Ho^{3+}) MC displays more high red-to-green (R/G) ratio.

The proposed UC mechanisms and energy level diagrams of Er^{3+}, Tm^{3+}, Ho^{3+}, and Yb^{3+} co-doped $LiYF_4$ and $LiLuF_4$ MCs are shown in Fig. 4(a–b) and briefly described as follows [35–39]: first, the electron of Yb^{3+} is excited from levels $^2F_{7/2}$ to $^2F_{5/2}$ under the 980 nm excitation. Then, the energy of the excited electron is transferred to Er^{3+}, Tm^{3+}, and Ho^{3+}. Through a two- or three-photon UC process, the ground-state electrons of Er^{3+}, Tm^{3+}, and Ho^{3+} are excited to $^2H_{9/2}$, $^2H_{11/2}$, $^4F_{9/2}$, $^1D_2$, $^1G_4$, $^5S_2$/$^5F_4$, and $^5F_3$ states. In the Yb^{3+}/Er^{3+} co-doped system, when the $^2H_{11/2}$/$^4S_{3/2}$ and $^4F_{9/2}$ states decay to ground $^5I_8$ state by radiative relaxation, the green and red UC emissions can be generated. In Yb^{3+}/Tm^{3+} co-doped system, the excited electrons of the $^1D_2$, $^1G_4$, and $^3H_4$ states decay to the levels of $^3F_4$ and $^3H_6$, resulting in blue (453 and 478 nm), red (650 nm), and NIR (800 nm) emission. In Yb^{3+}/Ho^{3+} co-doped $LiYF_4$ MCs, the strong green and weak red emission can be generated at the $^5S_2$/$^5F_4$ and $^5F_3$ state by radiative decays to ground $^5I_8$ state.

As can be seen from Fig. 3, the UC emission intensity of the single $LiLuF_4$ MC is stronger than the single $LiYF_4$ MC. To explore the main reason for the stronger UC emission in single $LiLuF_4$ MC, the site symmetry of the crystal field of $LiLuF_4$ and $LiLuF_4$ MCs is first discussed. The Eu^{3+} ion is regarded as a good probe for detecting site symmetry, which is because of the fact that the $^5D_0 \rightarrow {}^7F_1$ (591 nm) transition of Eu^{3+} is a magnetic nature dipole that is insensitive to site symmetry, whereas the $^5D_0 \rightarrow {}^7F_2$ (615 nm) transition of Eu^{3+} is an electric nature dipole that is very sensitive to site symmetry. Therefore, the ratio (η) of the emission intensity of $^5D_0 \rightarrow {}^7F_2$ and $^5D_0 \rightarrow {}^7F_1$ of Eu^{3+} is often used as a fingerprint of the local symmetry for luminescent centers [40,41]. The downconversion emission spectra of Yb^{3+}/Eu^{3+} co-doped single $LiYF_4$ and $LiLuF_4$ MC are shown in Fig. 5. The

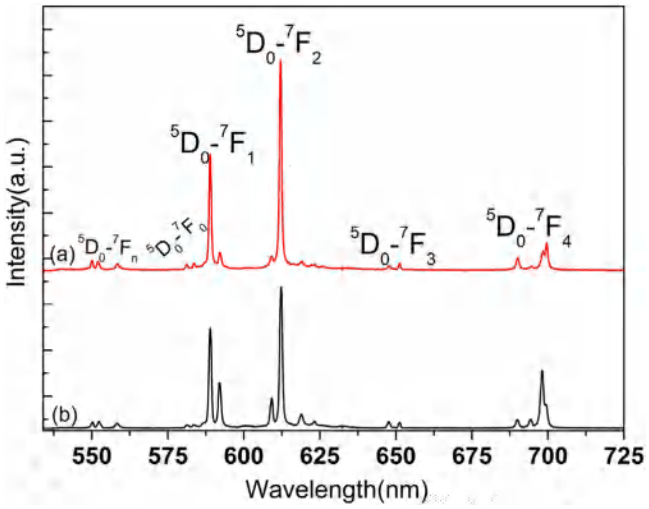

Fig. 5. Emission spectra of Eu^{3+} doped single $LiLuF_4$:Yb^{3+}/Eu^{3+} MC (a) and $LiYF_4$: Yb^{3+}/Eu^{3+} MC (b) under 532 nm excitation.

calculated η value increases from 1.27 to 1.39 when the host changes from $LiYF_4$ to $LiLuF_4$ MC. The result indicates the lower local symmetry around luminescence ions in $LiLuF_4$ MCs. According to J-O theory, the local symmetry is closely related to the Ω_2 intensity parameter; the lower local symmetry corresponds to the larger Ω_2 [42–44]. The larger Ω_2 leads to higher radiative transition probabilities of hypersensitive transitions for the luminescence ions, resulting in stronger UC emission. In addition, the ionic radius of Lu^{3+} (0.085 nm) is much closer to that of Yb^{3+} (0.086 nm) than Y^{3+} (0.089 nm) ions. Therefore, the Lu-based fluorides should be more stable for doping of Yb^{3+} with high concentration, which can effectively increase energy transfer rates from Yb^{3+} to luminescence ions.

In the $LiYF_4$ and $LiLuF_4$ MC synthesis process, the EDTA is employed as a chelator to control particle size and morphology. Some organic molecules may remain on the surface of the samples, which provide some extra pathways for the nonradiative relaxation of the UC states. Thus, the intensity difference for UC emission is possible due to the existence of EDTA on the surface of microparticles. Fourier-transform-infrared (FTIR) spectroscopy can help us to identify the existence of EDTA at the surface of microparticles. The observed $LiYF_4$ and $LiLuF_4$ FTIR spectra with

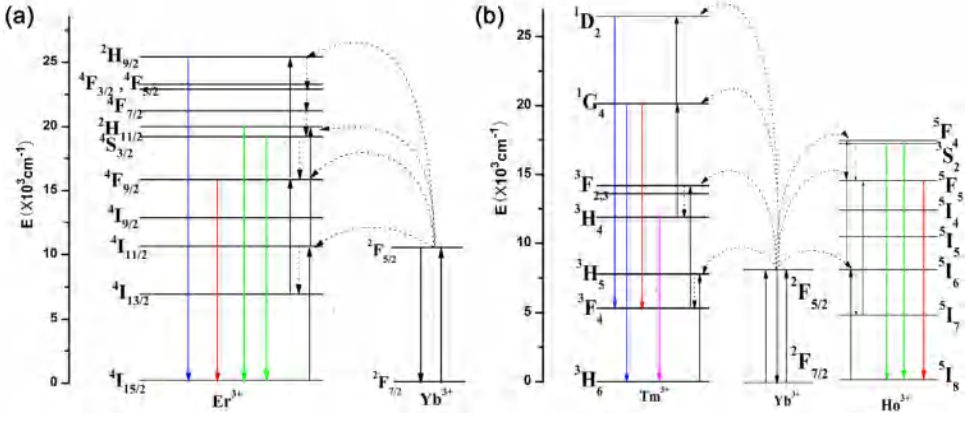

Fig. 4. Energy level diagrams with proposed UC mechanism for Er^{3+}, Tm^{3+}, Ho^{3+} and Yb^{3+} co-doped $LiYF_4$ MCs.

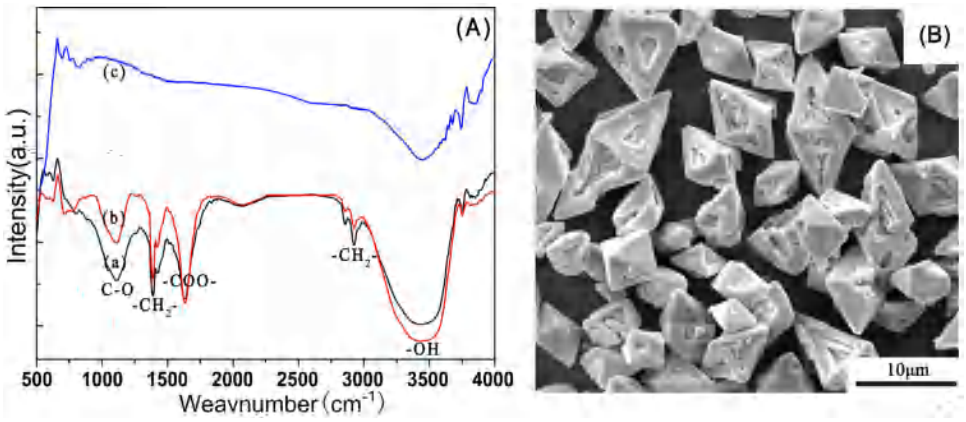

Fig. 6. (A) FTIR spectra of (a) $LiLuF_4$ and (b) $LiYF_4$ MCs in the presence of EDTA, and (c) $LiYF_4$ MCs in the absence of EDTA. (B) SEM images of $LiYF_4$ MCs in the absence of EDTA.

and without EDTA are presented in Fig. 6(A). The $-CH_2-$ (2850 cm^{-1}), $-CH_2-$ (1400 cm^{-1}), C—O (1091 cm^{-1}), and $-COO-$ (1640 cm^{-1}) stretching vibrations in the spectrum have been observed, and strong bands around 3400 cm^{-1} can be assigned to the $-OH-$ stretching vibrations of water and EDTA in Fig. 6(A(a) and(b) [33]. These results demonstrate that numerous EDTA exist on the surface of the $LiYF_4$ and $LiLuF_4$ MCs. Meanwhile, it can be found that the FTIR spectra intensity of the $LiYF_4$ MC is a little stronger than that of the $LiLuF_4$ MC. This result indicates that the more organic molecules derived from the EDTA on the surface of $LiYF_4$ MCs, resulting in nonradiative relaxation rate enhancement. Thus, the quenching of $LiYF_4$ MC UC emission intensity becomes more apparent than that of $LiYF_4$ MC ones. The high-energy vibrations from the $-OH-$ groups would strongly quench the excited states of Er^{3+}, Ho^{3+} ions and accelerate the multiphonon nonradiative relaxation processes of $^4I_{11/2} \rightarrow {}^4I_{13/2}$ and $^4S_{3/2} \rightarrow {}^4F_{9/2}$ of Er^{3+}, and $^5F_4/^5S_2 \rightarrow {}^5F_5$ and $^5I_6 \rightarrow {}^5I_7$ of Ho^{3+}, resulting in red emissions enhanced and green emission reduced, respectively [33,45,46]. Compared with the result of Fig. 6(A(a)), these obvious stretching vibrations cannot be found in the $LiYF_4$ MCs without no EDTA. The small $-OH-$ stretching vibration would arise from water. Fig. 6(B) displays the morphology of the $LiYF_4$ MCs with the synthesis process without EDTA. Some holes and defects are noticeable on the MC's surface. Obviously, several EDTA organic ligands exist on the MC surface, especially for face, leading to the higher R/G ratio of the Er^{3+} and Ho^{3+} ions in the single $LiYF_4$ MC.

3.3. UC emission of single $LiYF_4$ MC with different excitation positions

In order to further study the UC emission properties of single MC. We attempt to take a single $LiYF_4$: Yb^{3+}/Er^{3+} MC as an example. Fig. 7 shows the UC emission spectra and R/G ratio of different positions, including the apex, arris, and face of the single $LiYF_4$:Yb^{3+}/Er^{3+} MC under 980 nm excitation with a confocal microscopy setup. The UC emission intensity and the R/G ratio are different when the excitation position is changed in the single $LiYF_4$:Yb^{3+}/Er^{3+} MC. The UC emission intensity of the apex is stronger than the other positions in the single $LiYF_4$ MC; the R/G ratio of the face is highest. This result indicates that the UC emission intensity and R/G ratio can be tuned by changing the excitation position in the single $LiYF_4$ MC, which further extends their application in color display and micro-optoelectronic devices.

Although the concentrations of Y^{3+}, Yb^{3+}, and Er^{3+} in the solution are kept the same before each synthesis, the content of ions may be different in varying crystal positions. Hence, the element compositions and element ratios of the samples are confirmed by the EDX spectra in Fig. 8(a–d). The Y, Yb, and Er elemental contents of face are smallest, and the apex is highest in the single $LiYF_4$:Yb^{3+}/Er^{3+} MC. Thus, the UC emission intensity of

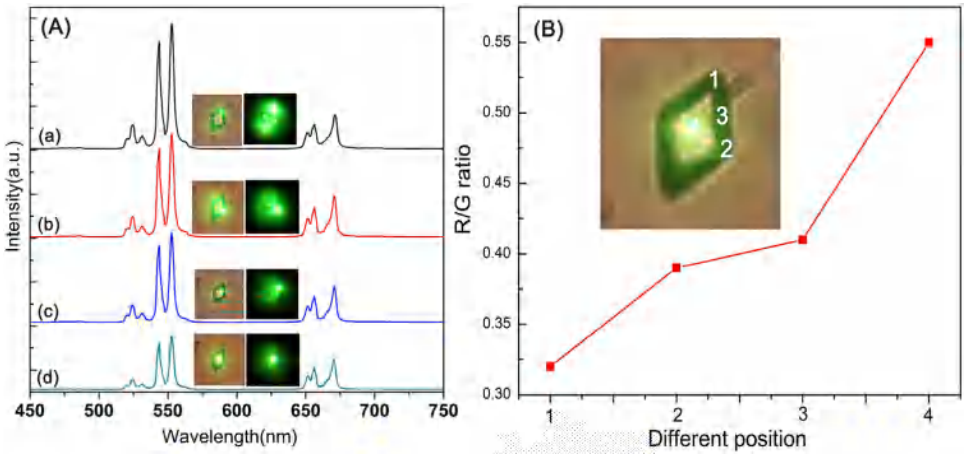

Fig. 7. (A) the UC emission spectra and (B) R/G ratio of single $LiYF_4$:Yb^{3+}/Er^{3+} MC with different excitation positions.

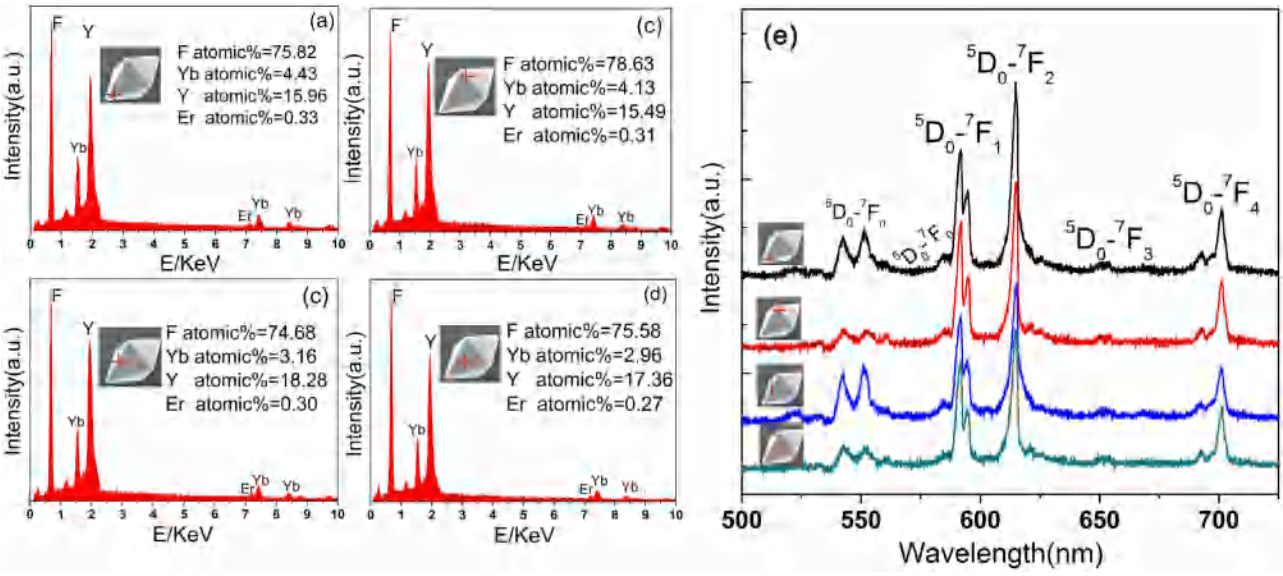

Fig. 8. (a–d) The EDX spectra of single $LiYF_4$:Yb^{3+}/Er^{3+} with different position. (e) The emission spectra of single $LiYF_4$:Yb^{3+}/Eu^{3+} MC with different position under 532 nm excitation.

the apex of the single $LiYF_4$:Yb^{3+}/Er^{3+} MC is strongest because more Yb^{3+} and Er^{3+} ions are included. In addition, the site symmetry of different excitation positions from the single $LiYF_4$:Yb^{3+}/Er^{3+} MC is investigated by introducing Eu^{3+} as a structure probe. The emission spectra of the different excitation positions of Yb^{3+}/Eu^{3+} co-doped single $LiYF_4$ MC is shown in Fig. 8(e). The calculated η values of the different excitation positions are 1.27 (apex), 1.21 (apex), 1.14 (arris), and 1.12 (face). Therefore, the effect of the excitation position on the UC emission of the single MC not only attributes to element compositions and element ratios but also originates from the site symmetry of luminescent ions. The different R/G ratio of the different excitation positions in single $LiYF_4$ MC is most probably ascribed to different amounts of organic ligands on the MC surface according to the result of Fig. 6(B).

4. Conclusions

Tetragonal octahedral $LiYF_4$ and $LiLuF_4$ MCs have been synthesized by a facile hydrothermal method. The strong blue, green, and red UC emissions of a single $LiYF_4$ and $LiLuF_4$ MC are observed by a confocal microscopy setup. The UC emission intensity of the single $LiLuF_4$ MC is stronger than that of the $LiYF_4$ MC. And the higher R/G ratio of Er^{3+} and Ho^{3+} can be obtained in single $LiYF_4$ MC. Meanwhile, when the excitation positions of single $LiYF_4$ was changed, the different emission intensities and R/G ratio can also be observed. The results indicated that the different UC emission intensity of single MC or different excitation position which is mainly due to different local site symmetry of crystal field. And the different R/G ratio is due to EDTA organic ligands on the MC surface. The current study suggests that the strong UC emission of single $LiYF_4$ and $LiLuF_4$ MC has great potential applications in multicolor display, micro-optoelectronic device.

Acknowledgements

This work was supported by the National Science Foundation of China (Grant No. 11604262, 11574190 and 11304247), Shaanxi Provincial Education Department (Program No.16JK1707), Shaanxi Provincial Research Plan for Young Scientific and Technological New Stars (Program No.2015KJXX-40), the New Star Team of Xi'an University of Posts & Telecommunications.

Appendix A. Supplementary data

Supplementary data associated with this article can be found, in the online version, at http://dx.doi.org/10.1016/j.materresbull.2017.03.043.

References

[1] F. He, P.P. Yang, D. Wang, C.X. Li, N. Niu, S.L. Gai, M.L. Zhang, Langmuir 27 (2011) 5616.
[2] Y.F. Bai, K. Yang, Y.X. Wang, X.R. Zhang, Y.L. Song, Opt. Commun. 281 (2008) 2930.
[3] X. Liang, X. Wang, J. Zhuang, Q. Peng, Y.D. Li, Adv. Funct. Mater. 17 (2007) 2757.
[4] J.C. Boyer, F. Vetrone, L.A. Cuccia, J.A. Capobianco, J. Am. Chem. Soc. 128 (2006) 7444.
[5] K. Kömpe, H. Borchert, J. Storz, A. Lobo, S. Adam, T. Möller, M. Haase, Angew. Chem. Int. Ed. 42 (2003) 5513.
[6] K. Riwotzki, M. Haase, J. Phys. Chem. B 102 (1998) 10129.
[7] R. Wang, Z. Yan, L. Huo, J. Wang, J. Zeng, X. Bao, Q. Peng Wang, Y. Li, Angew. Chem. Int. Ed. 44 (2005) 6054.
[8] A. Shalav, B.S. Richards, T. Trupke, K.W. Krämer, I.H.U. Güde, Appl. Phys. Lett. 86 (2005) 013505.
[9] Q. Liu, Y. Sun, T.S. Yang, W. Feng, C.G. Li, F.Y. Li, J. Am. Chem. Soc. 133 (2011) 17122.
[10] F. Zhang, Q.H. Shi, Y.C. Zhang, Y.F. Shi, K.L. Ding, D.Y. Zhao, G.D. Stucky, Adv. Mater. 23 (2011) 3775.
[11] X.Y. Huang, S.Y. Han, W. Huang, X.G. Liu, Chem. Soc. Rev. 42 (2013) 173.
[12] D.L. Gao, X.Y. Zhang, H.R. Zheng, W. Gao, E.J. He, J. Alloys. Compd. 554 (2013) 395.
[13] X.J. Pei, Y.B. Hou, S.L. Zhao, Z. Xu, F. Teng, Mater. Chem. Phys. 90 (2005) 270.
[14] S. Heer, K. Kompe, H.U. Gudel, M. Haase, Adv. Mater. 16 (2004) 2102.
[15] H.X. Mai, Y.W. Zhang, L.D. Sun, C.H. Yan, J. Phys. Chem. C 111 (2007) 13721.
[16] M.Y. Ding, C.H. Lu, L.H. Cao, Y.R. Ni, Z.Z. Xu, CrystEngComm 15 (2013) 8366.
[17] L.M. Wang, X.Y. Li, Z.Q. Li, W.S. Chu, R.F. Li, K. Lin, H.S. Qian, Y. Wang, C.F. Wu, J. Li, D.T. Tu, Q. Zhang, L. Song, J. Jiang, Adv. Mater. 27 (2015) 5528.
[18] P. Villanueva-Delgado, K.I.W. Krämer, R. Valiente, M. de Jong, A. Meijerink, Phys. Chem. Chem. Phys. 18 (2016) 27396.
[19] L. Lei, R. Wu, J. Zhou, S.J. Zhang, Z. Xiao, J.J. Zhang, S.Q. Xu, Mater. Lett. 189 (2017) 35.
[20] G.M. Bond, J.F. Browning, C.S.J. Snow, Appl. Phys. 107 (2010) 3514.
[21] F. Shi, J.S. Wang, X.S. Zhai, D. Zhao, W.P. Qin, CrystEngComm 13 (2011) 3782.
[22] J. Zhou, X.J. Zhu, M. Chen, Y. Sun, F.Y. Li, Biomaterials 33 (2012) 6201.
[23] K. Ogasawara, S. Watanabe, H. Toyoshima, T.M.G. Ishii, B.H. Ikeno, I.J. Tanaka, Solid State Chem. 178 (2005) 412.

[24] V. Mahalingam, F. Vetrone, R. Naccache, A. Speghini, J.A. Capobianco, Adv. Mater. 21 (2009) 4025.
[25] P.A. Rojas-Gutierrez, C. DeWolf, J.A. Capobianco, Part Part Syst. Charact. 12 (2016) 859.
[26] X.Y. Zhang, M.Q. Wang, J.J. Ding, J.P. Deng, C.X. Ran, Z. Yang, Dalton Trans. 43 (2014) 5453.
[27] J. Wang, F. Wang, J. Xu, Y. Wang, Y.S. Liu, X.Y. Chen, H.Y. Chen, X.G. Liu, C. R. Chimie 13 (2010) 731.
[28] M.Y. Ding, C.H. Lu, L.H. Cao, W.J. Huang, Y.R. Ni, Z.Z. Xu, CrystEngComm 15 (2013) 6015.
[29] G.Y. Chen, T.Y. Ohulchanskyy, A. Kachynski, H. Agren, P.N. Prasad, ACS Nano 5 (2011) 4981.
[30] J. Wang, F. Wang, J. Xu, Y. Wang, Y.S. Liu, X.Y. Chen, H.Y. Chen, X.G. Liu, C. R. Chimie 13 (2010) 731.
[31] J. Li, H.R. Zheng, W. Gao, E.J. He, D.L. Gao, Y. Tian, Chin. Sci. Bull. 57 (2012) 2366.
[32] W. Gao, H.R. Zheng, J. Li, D.L. Gao, E.J. He, Y.X. Tu, Sci. Sin. Phys. Mech. Astron. 10 (2012) 1.
[33] W. Gao, H.R. Zheng, E.J. He, Y. Lu, F.Q. Gao, J. Lumin. 152 (2014) 44.
[34] P. Huang, W. Zheng, S.Y. Zhou, D.T. Tu, Z. Chen, H.M. Zhu, R.F. Li, E. Ma, M.D. Huang, X.Y. Chen, Angew. Chem. Int. Ed. 53 (2014) 1252.
[35] D.L. Gao, X.Y. Zhang, W. Gao, J. Appl. Phys. 111 (2012) 033505.
[36] W. Gao, H.R. Zheng, Q.Y. Han, E.J. He, F.Q. Gao, R.B. Wang, J. Mater. Chem. C 2 (2014) 5327.
[37] J.J. Zhou, G.X. Chen, E. Wu, G. Bi, B.T. Wu, Y. Teng, S.F. Zhou, J.R. Qiu, Nano Lett. 13 (2013) 2241.
[38] Y.Y. Sun, W.Z. Wang, S.M. Sun, L. Zhang, Mater. Res. Bull. 52 (2014) 50.
[39] E.J. He, H.R. Zheng, W. Gao, Y.X. Tu, Y. Lu, G.A. Li, Mater. Res. Bull. 48 (2013) 3505.
[40] Q. Ju, Y.S. Liu, R.F. Li, L.Q. Liu, W.Q. Luo, X.Y. Chen, J. Phys. Chem. 113 (2009) 2309.
[41] D.L. Gao, H.R. Zheng, X.Y. Zhang, Z.X. Fu, Z.L. Zhang, Y. Tian, M. Cui, Appl. Phys. Lett. 98 (2011) 011907.
[42] B.R. Judd, Phys. Rev. 127 (1962) 750.
[43] G.S. Ofelt, J. Chem. Phys. 37 (1962) 511.
[44] R. Balda, J. Ferná ndez, M. Sanz, A. de Pablos, J.M. Fdez-Navarro, J. Mugnier, Phys. Rev. B 61 (2000) 3384.
[45] S. Wu, Y. Ning, J. Chang, W. Niu, S. Zhang, CrystEngComm 15 (2013) 3919.
[46] W. Gao, H.R. Zheng, Q.Y. Han, E.J. He, R.B. Wang, CrystEngComm 29 (2014) 6697.